Potential of observations from the Tropospheric Emission Spectrometer to constrain continental sources of carbon monoxide

JOURNAL OF GEOPHYSICAL RESEARCH, VOL. 108, NO. D24, 4789, doi:10.1029/2003JD003702, 2003

Potential of observations from the Tropospheric Emission Spectrometer to constrain continental sources of carbon monoxide

Dylan B. A. Jones,[1] Kevin W. Bowman,[2] Paul I. Palmer,[1] John R. Worden,[2] Daniel J. Jacob,[1] Ross N. Hoffman,[3] Isabelle Bey,[4] and Robert M. Yantosca[1]

Received 21 April 2003; revised 5 August 2003; accepted 25 August 2003; published 26 December 2003.

[1] We have conducted an observing system simulation experiment for the Tropospheric Emission Spectrometer (TES) satellite instrument to determine the potential of nadir retrievals of carbon monoxide (CO) from this instrument to constrain estimates of continental sources of CO. We use the GEOS-CHEM global chemical transport model to produce a pseudoatmosphere in which the relationship between sources and concentrations of CO is known. Linear profile retrievals of CO are calculated by sampling this pseudoatmosphere along the orbit of TES. These retrievals are used as pseudo-observations with a maximum a posteriori inverse algorithm to estimate the CO sources from the different continents. This algorithm accounts for the finite vertical resolution of the retrieval, instrument errors, and representation and transport errors in the GEOS-CHEM simulation of CO. The structure of the transport error is estimated using the statistics of the difference between paired GEOS-CHEM forecasts of CO, and this structure is then scaled to match the model error in the GEOS-CHEM simulation of aircraft observations of Asian outflow over the NW Pacific. We show that with proper characterization of observation errors just 2 weeks of observations from TES have the potential to constrain estimates of continental sources of CO to within 10%. *INDEX TERMS:* 0322 Atmospheric Composition and Structure: Constituent sources and sinks; 0365 Atmospheric Composition and Structure: Troposphere—composition and chemistry; 0368 Atmospheric Composition and Structure: Troposphere—constituent transport and chemistry; *KEYWORDS:* TES, carbon monoxide, inverse methods

Citation: Jones, D. B. A., K. W. Bowman, P. I. Palmer, J. R. Worden, D. J. Jacob, R. N. Hoffman, I. Bey, and R. M. Yantosca, Potential of observations from the Tropospheric Emission Spectrometer to constrain continental sources of carbon monoxide, *J. Geophys. Res.*, *108*(D24), 4789, doi:10.1029/2003JD003702, 2003.

1. Introduction

[2] Accurate estimates of the sources of atmospheric carbon monoxide (CO) are essential to understand the impact of human activity on the composition of the atmosphere. Atmospheric CO is a product of incomplete combustion and a by-product of the oxidation of atmospheric hydrocarbons. It plays a critical role in determining the oxidative capacity of the atmosphere because it is the primary sink of OH, the main tropospheric oxidant. Present estimates of the sources of CO derived from inventory-based, bottom-up techniques are highly uncertain. Recently, a number of studies have used a top-down approach employing inverse modeling techniques with atmospheric observations of CO to better constrain estimates of the sources [e.g., *Bergamaschi et al.*, 2000a, 2000b; *Kasibhatla et al.*, 2002; *Pétron et al.*, 2002; *Palmer et al.*, 2003]. These studies relied on data from aircraft campaigns or surface observation sites with limited spatiotemporal coverage. Global observations of CO from satellite instruments such as the Measurement of Air Pollution from Space (MAPS) [*Reichle et al.*, 1999; *Lamarque et al.*, 1999], the Interferometric Monitor of Greenhouse Gases (IMG) [*Clerbaux et al.*, 2001], and the Measurements of Pollution in the Troposphere (MOPITT) [*Drummond and Mand*, 1996] offer new constraints on CO sources. The Tropospheric Emission Spectrometer (TES), scheduled for launch in 2004 on the Aura spacecraft, will provide augmented resolution of the vertical profile of CO using spectrally resolved infrared measurements of CO absorption lines around the 4.7-μm band [*Beer et al.*, 2001].

[3] In this study we examine quantitatively the potential of nadir observations from TES to constrain estimates of continental sources of CO. The addition of limb observations should provide additional vertical and angular information on the CO distribution. However, this is one of the first studies to examine the utility of space-based observations for constraining estimates of CO sources. We believe

[1]Division of Engineering and Applied Sciences and Department of Earth and Planetary Sciences, Harvard University, Cambridge, Massachusetts, USA.
[2]California Institute of Technology, Jet Propulsion Laboratory, Pasadena, California, USA.
[3]Atmospheric and Environmental Research, Inc., Lexington, Massachusetts, USA.
[4]Swiss Federal Institute of Technology, Lausanne, Switzerland.

0148-0227/03/2003JD003702

that the first-order task should be to establish the utility of observations from the nadir or limb mode separately, before attempting to combine the two data sets. Combining the limb and nadir retrievals and properly accounting for the different sensitivities of these two modes of observation and the possible covariance of retrieval errors will be a challenging task. In particular, the vertical and angular distribution of atmospheric temperature and constituents along with cloud top heights must be taken into account for limb retrievals. Therefore for simplicity we focus on nadir retrievals here and we will consider limb retrievals in a subsequent study. We use the GEOS-CHEM global three-dimensional model of tropospheric chemistry [*Bey et al.*, 2001a; *Duncan et al.*, 2003; B. N. Duncan et al., Model study of the variability and trends in carbon monoxide (1988–1997): 1. Model formulation, evaluation, and sensitivity, submitted to *Journal of Geophysical Research*, 2003 (hereinafter referred to as Duncan et al., submitted manuscript, 2003)] to produce a pseudoatmosphere in which the relationships between sources and concentrations of CO are known exactly. Vertical, linear profile retrievals of CO are calculated by sampling this pseudoatmosphere along the orbit of TES. The resulting profiles provide a pseudo–data set of TES observations. We then examine the ability of these observations to constrain CO source estimates by using a maximum a posteriori (MAP) inverse algorithm [*Rodgers*, 2000], starting from an a priori estimate of the sources. Our goal is to determine if the pseudo-observations from TES contain sufficient information to accurately estimate the specified "true" source strengths, given the vertical resolution of the TES retrieval, instrument noise, and associated forward model errors.

[4] Characterizing errors in the observations and forward model is a critical issue in inverse modeling. *Palmer et al.* [2003] showed that transport errors in the forward model can be the largest source of uncertainty in an inversion analysis of atmospheric CO and presented a method to estimate the statistics of these errors through simulation of aircraft observations. We extend this approach here to the global scale by using pairs of successive chemical forecasts of CO generated with the GEOS-CHEM model, as described below.

[5] We begin with a description of the TES instrument in section 2. We discuss our approach for generating the CO retrievals in section 3. The inversion methodology and the characterization of forward model transport and representation errors are presented in section 4. The a posteriori CO source strengths and their error covariance are discussed in section 5. In section 6 we present a summary of the results and a discussion of their implications for the potential of observations from TES.

2. TES Instrument

2.1. TES Description

[6] The TES instrument is an infrared Fourier transform spectrometer that measures thermal emission from atmospheric trace gases over the spectral range 650–2250 cm^{-1} (4.4–15.4 μm) [*Beer et al.*, 2001]. It will be launched on board the Aura spacecraft in 2004 into a Sun-synchronous orbit at an altitude of 705 km, with an inclination of 98.2°, and with a 1345 LT (local mean solar) equator crossing time. The Aura spacecraft will make 14.56 orbits per day, with the orbits repeating every 16 days (233 orbits). The instrument will operate in both nadir and limb modes and will make 73 observations per orbit with a 1-day-on, 1-day-off observational cycle. In the limb mode of observation each of the 16 detectors on TES will view the limb with a different tangent height. In the nadir mode the combined footprint of this 16-detector array will be 5 km across-track by 8 km along-track, with each detector observing a field of view of 5 km × 0.5 km. The observations will be spaced by about 5° along the orbit track.

2.2. Nadir Retrievals of CO

[7] A detailed discussion of the nonlinear retrieval of vertical profiles of trace gases using TES radiances is presented by *Clough et al.* [2002] and *Bowman et al.* [2002]. The dependence of the retrieved profile of CO on the true state can be approximated by the linear relation [*Rodgers*, 2000]

$$\hat{\mathbf{y}}^j = \mathbf{y}_a + \mathbf{A}_{yy}(\mathbf{y}^j - \mathbf{y}_a) + \mathbf{G}_y\mathbf{n}, \tag{1}$$

where $\hat{\mathbf{y}}^j \in \mathbb{R}^N$ is the retrieval vector (for a given spatiotemporal location j) whose elements are the natural log of the volume mixing ratio of CO, N is the number of pressure levels in the profile ($N \approx 28$ and represents a subset of the 87 levels of the pressure grid of the TES radiative transfer forward model [*Clough and Iacono*, 1995; *Clough et al.*, 1995]), $\mathbf{y}^j \in \mathbb{R}^N$ is the true profile, $\mathbf{y}_a \in \mathbb{R}^N$ is the a priori constraint vector, $\mathbf{n} \in \mathbb{R}^M$ is the spectral radiance noise vector of M spectral elements, $\mathbf{G}_y \in \mathbb{R}^{N\times M}$ is the gain matrix, and $\mathbf{A}_{yy} \in \mathbb{R}^{N\times N}$ is the averaging kernel matrix. For simplicity, the linear retrieval described by equation (1), together with a representative averaging kernel matrix, is used to generate the pseudo–data set of CO profiles for this study.

[8] The averaging kernel matrix $\mathbf{A}$ describes the sensitivity of the retrieved profile to perturbations of the true profile. The rows of the averaging kernel matrix are shown in Figure 1a. Each row of the averaging kernel matrix describes the change in the retrieved state at a specific pressure level to a perturbation of the true state vector. The degrees of freedom for signal (dofs), which is a measure of the number of independent elements of the retrieved state [*Rodgers*, 2000], is calculated by

$$\text{dofs} = \text{tr}(\mathbf{A}_{yy}). \tag{2}$$

The dofs for the averaging kernel in Figure 1a is 2.1, which reflects the strong correlation in the retrieved CO between the levels below about 600 hPa and between levels above 500 hPa.

[9] The retrieval spectral noise error is the last term in equation (1). The spectral radiance noise vector, $\mathbf{n}$, is assumed to be zero-mean, white Gaussian noise such that

$$\mathbf{S}_n^j = E[\mathbf{n}\mathbf{n}^T] = \sigma^2\mathbf{I}, \tag{3}$$

where $E[\cdot]$ is the expectation operator [*Papoulis*, 1984] and $\sigma = 3.8 \times 10^{-9}$ W cm^{-2} sr^{-1}/cm^{-1} is the noise equivalent spectral radiance (NESR) averaged over all detectors. The

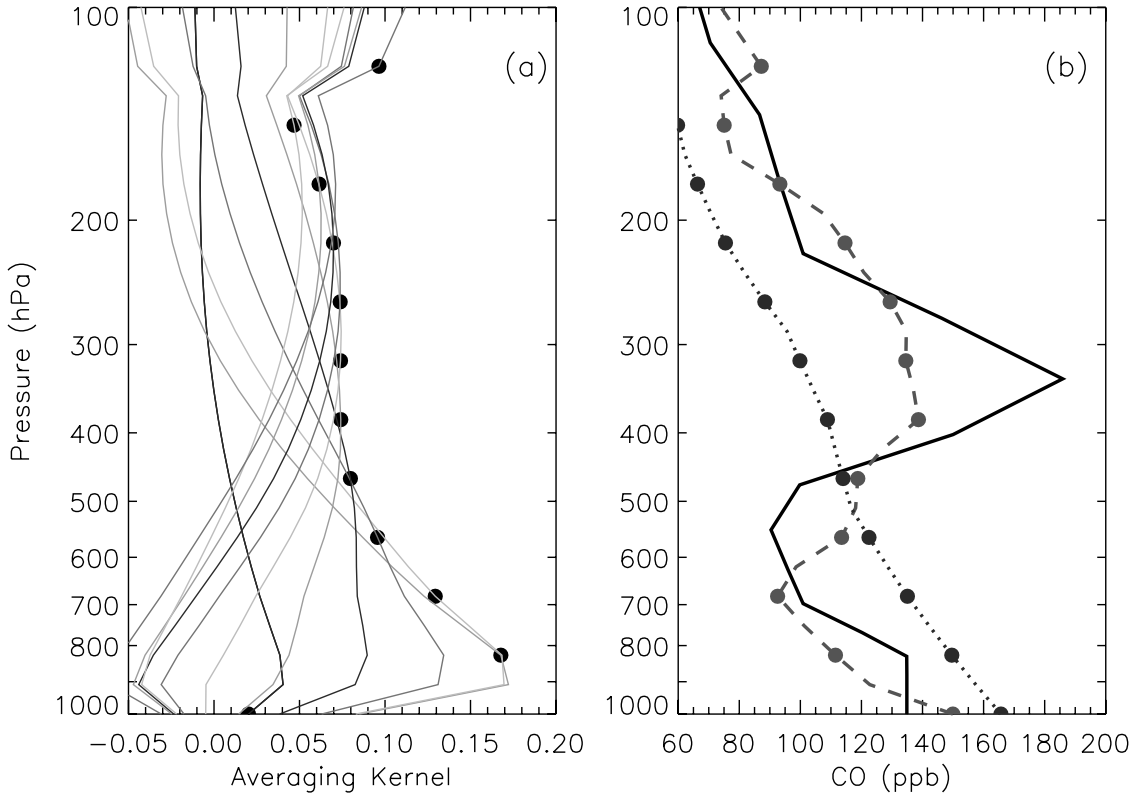

Figure 1. (a) Averaging kernels for TES nadir retrieval of CO for selected retrieval levels between 1000 and 100 hPa. The corresponding retrieval levels for the individual averaging kernels are indicated by solid circles. (b) Example of a retrieved profile. The true profile is represented by the solid line, the a priori profile is shown by the dotted line, and the retrieved profile is denoted by the dashed line. The retrieval levels are indicated by the solid circles. See color version of this figure at back of this issue.

retrieval spectral noise error or instrument error covariance matrix is calculated by combining equations (3) and (1),

$$\mathbf{S}_{\text{ret}}^{j} = \mathbf{G}_y \mathbf{S}_n^{j} (\mathbf{G}_y)^T. \quad (4)$$

Other sources of observation error are discussed in section 4.2.

3. Generating the Pseudo-Observations

3.1. GEOS-CHEM Model

[10] The GEOS-CHEM model is a global three-dimensional chemical transport model (CTM) driven by assimilated meteorological observations from the Goddard Earth Observing System (GEOS) of the NASA Data Assimilation Office (DAO). A detailed description of the model, along with a comparison of model results with observations, is presented by *Bey et al.* [2001a]. Recent applications of GEOS-CHEM to the simulation of CO are presented in the work of *Duncan et al.* [2003], B. N. Duncan et al. (submitted manuscript, 2003), *Palmer et al.* [2003], and *Heald et al.* [2003a, 2003b]. We employ here version 4.20 of GEOS-CHEM (http://www-as.harvard.edu/chemistry/trop/geos), driven by GEOS-3 assimilated meteorological fields for 2000 and 2001. The model has a horizontal resolution of $2^\circ \times 2.5^\circ$ with 48 sigma levels in the vertical from the surface to 0.01 hPa. In our simulation of CO we use the CO-only mode of GEOS-CHEM [*Bey et al.*, 2001b], in which the loss of CO due to reaction with OH is calculated from archived monthly mean concentrations of OH.

[11] Global sources of CO used here are based on the source inventories of Duncan et al. (submitted manuscript, 2003) and *Yevich and Logan* [2003]. We use source estimates appropriate for 1994. The global, annual source strength is 2270 Tg CO. Emissions of CO from biomass burning and from the combustion of fossil fuels and biofuels together contribute about 50% of that total. The remaining is from photochemical oxidation of methane and nonmethane volatile organic compounds. Biomass burning sources are specified on a monthly mean basis and have a strong seasonal variation [*Duncan et al.*, 2003]. We assume that emissions of CO from biofuel and fossil fuel combustion are aseasonal.

3.2. Pseudo-Observation Data Set

[12] We generate TES retrievals of CO for February–April 2001, during the period of the NASA Transport and Chemical Evolution over the Pacific (TRACE-P) aircraft campaign [*Jacob et al.*, 2003]. The TRACE-P campaign was conducted off the eastern coast of Asia to study the outflow of Asian pollution over the western Pacific Ocean. We focus on this period because the TRACE-P aircraft observations of CO provide valuable data to characterize the forward model transport error in the inversion analysis [*Palmer et al.*, 2003; see also section 4.2]. The TES

Table 1. CO Source Categories Used in the Inverse Model Analysis

Source[a]	Symbol	"True" CO Emissions, Tg CO/yr
North American fuel combustion	NAFFBF	121
European fuel combustion	EUFFBF	131
Asian fuel combustion	ASFFBF	258
Asian biomass burning	ASBB	96
African biomass burning	AFBB	194
South American biomass burning	SABB	96
Rest of the world biomass burning[b]	RWBB	98
Rest of the world fuel combustion[c]	RWFFBF	150
Chemical production[d]	CHEM	1125
Total		2269

[a]Fossil fuel, biofuel, and biomass burning sources include a secondary contribution of CO from the oxidation of nonmethane hydrocarbons emitted by these sources.

[b]RWBB includes major contributions from biomass burning in North America, Central America, Indonesia, and Australia.

[c]RWFFBF includes major contributions from fossil fuel and biofuel combustion in Central America, South America, Africa, Indonesia, and Australia.

[d]CHEM represents the production of CO from the oxidation of methane and biogenic nonmethane volatile organic compounds.

retrievals are produced by sampling the pseudoatmosphere along the TES orbit [*Beer et al.*, 2001]. We assume that each 5 km × 8 km nadir measurement is representative of the entire 2° × 2.5° GEOS-CHEM grid box within which it falls; this approach introduces representation error but no artifact covariance since the measurements are spaced by about 5°. We restrict the coverage of the retrievals here to observations between the equator and 60°N (about 25 out of the 73 observations per orbit) which are most useful for our purpose. The effects of clouds are included, following *Luo et al.* [2002]. We assume that clouds are randomly distributed within a given GEOS-CHEM grid box with a uniform distribution and that the GEOS-3 cloud fraction for the grid box represents the probability that the TES retrieval will be contaminated by cloud cover. We exclude all retrievals which contain cloudy scenes, resulting in a loss of about 60% of the retrievals (see Figure 1 of *Luo et al.* [2002]).

[13] Retrieved vertical profiles are produced by first interpolating the "true" vertical profiles of CO from GEOS-CHEM onto the TES pressure levels and then substituting these profiles into equation (1). An example of a retrieved profile from the northwestern Pacific is shown in Figure 1b. The true profile in Figure 1b shows enhanced CO in the upper troposphere from biomass burning in Southeast Asia as simulated by the GEOS-CHEM model. The retrieved profile captures some of this biomass burning signal in the upper troposphere and the low concentrations of CO in lower troposphere.

4. Inversion Methodology

[14] The pseudo-observations are incorporated into a maximum a posteriori inverse model to quantify the sources of CO, which are aggregated here into nine source categories (listed in Table 1). The corresponding geographical regions for the sources are shown in Figure 2. The subregional distribution and the seasonal cycle of the sources are specified as a priori constraints; the inversion adjusts the source strengths but does not modify their spatial distribution or their seasonal variability. In our analysis we combine fossil fuels and biofuel sources. These sources of CO are spatially coincident and consequently cannot be independently resolved by the inversion analysis [*Kasibhatla et al.*, 2002; *Palmer et al.*, 2003]. The a priori is constructed by randomly perturbing the "true" source strengths (defined in Table 1). We assume that the sources are uncorrelated and have a uniform a priori error of 50%. Our analysis quantifies the sources for the February–April 2001 period; however, for clarity we express the source estimates as annual means

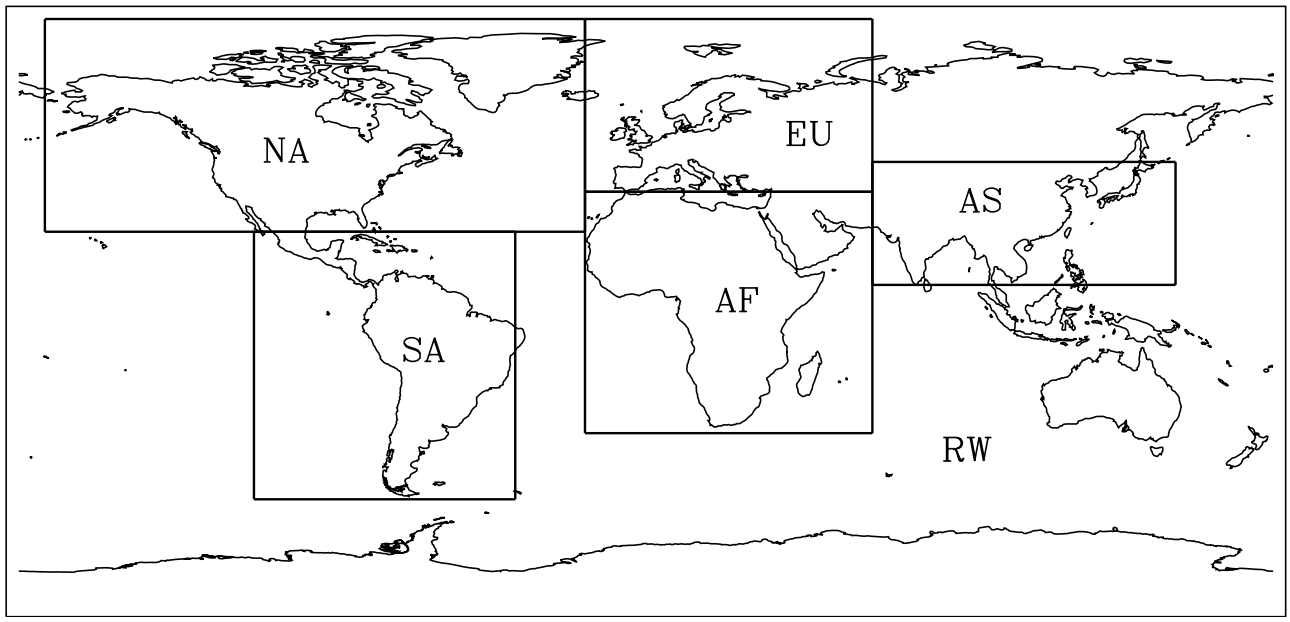

Figure 2. Regions for sources of CO specified in the state vector of the inversion analysis. The sources are described in Table 1. The regions indicated are North America (NA), South America (SA), Europe (EU), Africa (AF), and Asia (AS). All other areas are included in the rest of the world (RW) region.

by assuming that the a priori seasonal cycle of the sources is correct.

4.1. Maximum A Posteriori Method

[15] A retrieved profile at a specific spatiotemporal location j can be related to the sources of CO as

$$\hat{\mathbf{y}}^j = \mathbf{F}^j(\mathbf{x}) + \boldsymbol{\varepsilon}^j, \tag{5}$$

where $\mathbf{x} \in \mathbb{R}^n$ is the state vector whose elements are the sources of CO for the regions and source types listed in Table 1 ($n = 9$ is the number of elements in the state vector), $\hat{\mathbf{y}}^j \in \mathbb{R}^N$ is the retrieved profile of CO (given by equation (1)), and $\boldsymbol{\varepsilon}^j \in \mathbb{R}^N$ is the observation error. The forward model $\mathbf{F}^j$: $\mathbb{R}^n \rightarrow \mathbb{R}^N$ transforms the CO sources into concentrations of CO through the GEOS-CHEM model and accounts for the vertical sensitivity of TES and the a priori constraints used in the TES retrievals. The expression for the forward model is thus analogous to equation (1),

$$\mathbf{F}^j(\mathbf{x}) = \mathbf{y}_a + \mathbf{A}_{yy}\left(\ln\left[\mathbf{H}^j(\mathbf{x})\right] - \mathbf{y}_a\right), \tag{6}$$

where $\mathbf{H}^j$: $\mathbb{R}^n \rightarrow \mathbb{R}^N$ represents the GEOS-CHEM model, and the a priori vector and averaging kernel are defined in equation (1).

[16] The observation error $\boldsymbol{\varepsilon}^j$ is composed of errors from the retrievals, representation errors, and GEOS-CHEM model errors

$$\boldsymbol{\varepsilon}^j = \boldsymbol{\varepsilon}^j_{\text{ret}} + \boldsymbol{\varepsilon}^j_{\text{rep}} + \boldsymbol{\varepsilon}^j_{\text{mod}} = \boldsymbol{\varepsilon}^j_{\text{ret}} + A_{yy}\left(\boldsymbol{\varepsilon}'^j_{\text{rep}}\right) + A_{yy}\left(\boldsymbol{\varepsilon}'^j_{\text{mod}}\right), \tag{7}$$

where $\boldsymbol{\varepsilon}_{\text{ret}}{}^j = \mathbf{G}_y\mathbf{n}$ is the retrieval error specified in equation (1), $\boldsymbol{\varepsilon}'^j_{\text{rep}}$ and $\boldsymbol{\varepsilon}'^j_{\text{mod}}$ are the representation errors and GEOS-CHEM transport errors, respectively, in the GEOS-CHEM vertical coordinates, and $\boldsymbol{\varepsilon}^j_{\text{rep}}$ and $\boldsymbol{\varepsilon}^j_{\text{mod}}$ are the ''smoothed'' representation errors and model transport errors, respectively. These terms are considered ''smoothed'' because they include the effects of the averaging kernels from the TES retrieval. We assume here that the observation error $\boldsymbol{\varepsilon}^j$ is zero-mean and has a Gaussian distribution with respect to the logarithm of the volume mixing ratio of CO. We also assume that the errors that comprise $\boldsymbol{\varepsilon}^j$ are uncorrelated. The observation error covariance is

$$\mathbf{S}^j_{\varepsilon} = E[(\boldsymbol{\varepsilon}^j)(\boldsymbol{\varepsilon}^j)^T] = \mathbf{S}^j_{\text{ret}} + \mathbf{S}^j_{\text{rep}} + \mathbf{S}^j_{\text{mod}}, \tag{8}$$

where $\mathbf{S}^j_{\text{ret}} \in \mathbb{R}^{N\times N}$ is the instrument error covariance matrix (given by equation (4)), $\mathbf{S}^j_{\text{rep}} \in \mathbb{R}^{N\times N}$ is the representation error covariance matrix, and $\mathbf{S}^j_{\text{mod}} \in \mathbb{R}^{N\times N}$ is the forward model transport error covariance matrix. The representation error covariance matrix and the forward model transport error covariance matrix are given by

$$\mathbf{S}^j_{\text{rep}} = E\left[\left(\boldsymbol{\varepsilon}^j_{\text{rep}}\right)\left(\boldsymbol{\varepsilon}^j_{\text{rep}}\right)^T\right] = \mathbf{A}_{yy}E\left[\left(\boldsymbol{\varepsilon}'^j_{\text{rep}}\right)\left(\boldsymbol{\varepsilon}'^j_{\text{rep}}\right)^T\right]\mathbf{A}^T_{yy} \tag{9}$$

and

$$\mathbf{S}^j_{\text{mod}} = E\left[\left(\boldsymbol{\varepsilon}^j_{\text{mod}}\right)\left(\boldsymbol{\varepsilon}^j_{\text{mod}}\right)^T\right] = \mathbf{A}_{yy}E\left[\left(\boldsymbol{\varepsilon}'^j_{\text{mod}}\right)\left(\boldsymbol{\varepsilon}'^j_{\text{mod}}\right)^T\right]\mathbf{A}^T_{yy}. \tag{10}$$

[17] We obtain an optimal estimate of the sources of CO from the pseudo-observations of CO by minimizing the MAP cost function [*Rodgers*, 2000]

$$\mathrm{J}(\mathbf{x}) = (\hat{\mathbf{y}} - \mathbf{F}(\mathbf{x}))^T\mathbf{S}^{-1}_{\varepsilon}(\hat{\mathbf{y}} - \mathbf{F}(\mathbf{x})) + (\mathbf{x} - \mathbf{x}_a)^T\mathbf{S}^{-1}_a(\mathbf{x} - \mathbf{x}_a), \tag{11}$$

where $\hat{\mathbf{y}} \in \mathbb{R}^m$ is the observation vector whose elements are the retrievals of CO described in equation (1) (we concatenate retrieved profiles between the surface and 250 hPa), m is total number of observations used in the inversion analysis (about 2000 observations per day, depending on the fraction of retrievals lost due to cloud cover), $\mathbf{S}_{\varepsilon} \in \mathbb{R}^{m\times m}$ is the block diagonal error covariance matrix of the observation vector (with each block given by the matrix $\mathbf{S}^j_{\varepsilon}$, defined in equation (8)). As previously defined, $\mathbf{x} \in \mathbb{R}^n$ is the state vector whose elements are the strengths of the sources of CO for the regions and source types listed in Table 1, and $\mathbf{F}(\mathbf{x}) \in \mathbb{R}^m$ is the forward model whose elements are defined in equation (6). The quantity $\mathbf{x}_a \in \mathbb{R}^n$ is the a priori state vector and $\mathbf{S}_a \in \mathbb{R}^{n\times n}$ is the a priori covariance matrix. $\mathbf{S}_a$ is diagonal, since, as described above, we assume that the sources are uncorrelated (with uniform uncertainty of 50%). The a posteriori estimate of the state vector is obtained by iteratively minimizing the cost function in equation (11). For the Gauss-Newton method [*Rodgers*, 2000] a single iteration is

$$\mathbf{x}_{i+1} = \mathbf{x}_i + \left(\mathbf{K}^T_i\mathbf{S}^{-1}_{\varepsilon}\mathbf{K}_i + \mathbf{S}^{-1}_a\right)^{-1} \cdot \left[\mathbf{K}^T_i\mathbf{S}^{-1}_{\varepsilon}(\hat{\mathbf{y}} - \mathbf{F}(\mathbf{x}_i)) - \mathbf{S}^{-1}_a(\mathbf{x}_i - \mathbf{x}_a)\right], \tag{12}$$

where $\mathbf{x}_i$ and $\mathbf{K}_i = \partial\mathbf{F}(\mathbf{x}_i)/\partial\mathbf{x} \in \mathbb{R}^{m\times n}$ are estimates of the state vector and the Jacobian matrix, respectively, at the ith iteration. To reduce the computational costs associated with manipulating the matrices in equation (12), we use a sequential approach for each iteration in which the inversion model ingests one retrieved profile at a time. This sequential updating technique is described in Appendix A.

[18] Despite the linearity of the chemistry (as a result of the specified OH abundances), the forward model is nonlinear with respect to $\mathbf{x}$ because CO fields are expressed in terms of the natural logarithm of the mixing ratio of CO for the TES retrievals. Therefore we must recalculate the Jacobian matrix at each iteration. The Jacobian for the jth profile ingested during the ith iteration is given by

$$\mathbf{K}^j_i = \frac{\partial\mathbf{F}^j(\mathbf{x}_i)}{\partial\mathbf{x}} = \frac{\mathbf{A}_{yy}\partial\ln[\mathbf{H}^j(\mathbf{x}_i)]}{\partial\mathbf{x}} = \mathbf{A}_{yy}\left[\frac{1}{\mathbf{H}^j(\mathbf{x}_i)}\left(\frac{\partial\mathbf{H}^j(\mathbf{x}_i)}{\partial\mathbf{x}}\right)\right]. \tag{13}$$

The quantity $\partial\mathbf{H}^j(\mathbf{x}_i)/\partial\mathbf{x}$ is the sensitivity of the concentration of CO to the sources. We calculate $\partial\mathbf{H}^j(\mathbf{x}_i)/\partial\mathbf{x}$ using a ''tagged CO'' approach in GEOS-CHEM in which we specify a separate CO tracer for each source; the sensitivity of the CO concentration to a particular source is thus given by the abundance of the tagged CO from that source divided by the magnitude of the source.

[19] We assume convergence in equation (12), following *Rodgers* [2000], with the error criterion

$$(\mathbf{x}_i - \mathbf{x}_{i+1})^T \left(\mathbf{K}_i^T \mathbf{S}_\varepsilon^{-1} \mathbf{K}_i + \mathbf{S}_a^{-1}\right)^{-1} (\mathbf{x}_i - \mathbf{x}_{i+1}) < 0.1. \quad (14)$$

Convergence is typically achieved in 3–4 iterations. The a posteriori error covariance matrix is given by

$$\hat{\mathbf{S}} = (\hat{\mathbf{K}}^T \mathbf{S}_\varepsilon^{-1} \hat{\mathbf{K}} + \mathbf{S}_a^{-1})^{-1}, \quad (15)$$

where $\hat{\mathbf{K}}$ is the Jacobian matrix calculated for the a posteriori estimate of the state vector.

4.2. Forward Model Error Specification

[20] The a posteriori estimate of the sources depends critically on the observation error covariance matrix $\mathbf{S}_\varepsilon$. *Palmer et al.* [2003] showed that forward model transport errors can be the dominant component in $\mathbf{S}_\varepsilon$, with representation errors providing a much smaller contribution. We present here a brief description of the representation errors and a methodology for characterizing the forward model transport errors that contribute to $\mathbf{S}_\varepsilon$.

[21] Representation errors arise because the TES nadir measurements have a 5 km × 8 km footprint that may not be representative of the mean concentrations of CO over the 2° × 2.5° GEOS-CHEM grid. We adopt here a uniform representation error of 5% based on the estimates by *Palmer et al.* [2003] of the subgrid-scale variance of aircraft observations of CO over the NW Pacific.

[22] The forward model error represents uncertainties in model parameters affecting the relationship between the sources and concentrations of CO. It includes contributions from the simulation of transport, the specification of OH concentrations, and the assumed distribution of the sources of CO within the regions of Figure 1. *Palmer et al.* [2003] estimated this error in their inversion analysis of TRACE-P observations of CO by calculating the relative differences between the observations and the GEOS-CHEM model along the aircraft flight tracks. They postulated that the mean relative differences (i.e., mean bias) were due to errors in the a priori CO sources and that the residual defined the model errors, mainly from transport. They verified the validity of the approach by finding that the a posteriori source estimates from their inversion significantly reduced the mean bias but had little effect on the residual error. We adopt here the model errors calculated as a function of altitude by *Palmer et al.* [2003] using their a posteriori source estimates. These errors are typically 20–30%.

[23] The *Palmer et al.* [2003] analysis defines model errors specific to the NW Pacific as observed in the TRACE-P mission. To extrapolate to the entire hemisphere we first use the "NMC method" [*Parish and Derber*, 1992] to describe the global transport error patterns in the model. In the NMC method it is assumed that differences between forecasts for the same end time, but of different lengths, are representative of the forecast error structure (in our analysis, the error structure in the transport of CO). This method was originally developed for data assimilation of meteorological variables [e.g., *Parish and Derber*, 1992; *Rabier et al.*, 1998]. We construct the forecast error covariance over the Northern Hemisphere by using differences between 89 pairs of 48- and 24-hour forecasts of CO that were generated for 3 months (February–April 2001) during the TRACE-P campaign with the GEOS-CHEM model, driven by meteorological forecasts from the same meteorological model (GEOS-3) as is used here. A detailed discussion of this approach and the estimated model error covariance is presented by D. B. A. Jones et al. (manuscript in preparation, 2003). The forecast error covariance estimated using the NMC method reflects the dominant mode of growth, over the 24-hour period, of the errors associated with the differences in the initial conditions of the forecasts. They are not necessarily representative of the actual magnitude of the errors in the forecast model. Consequently, in data assimilation the variances are usually scaled using an empirically derived global scaling factor [e.g., *Rabier et al.*, 1998; *Derber and Bouttier*, 1999]. In our application where transport errors could accumulate and where other sources of error could be present (e.g., from regional source patterns not resolved by the model), scaling of the forecast errors is also necessary.

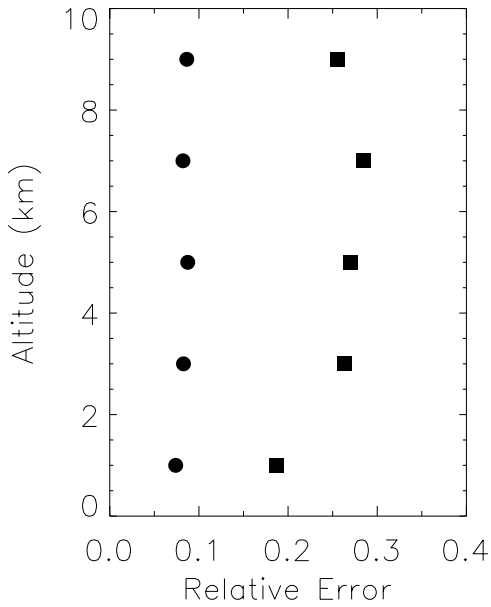

Figure 3. Comparison of the relative model error (squares) [from *Palmer et al.*, 2003] and the mean relative forecast errors (circles), as a function of altitude, for the NW Pacific region sampled by the TRACE-P aircraft.

[24] We estimate scaling factors by calculating the mean forecast errors from the NMC method for all the GEOS-CHEM grid boxes sampled by the TRACE-P aircraft in the domain considered by *Palmer et al.* [2003], binned into 2-km altitude bins, and comparing them with the model errors from the work of *Palmer et al.* [2003]. As shown in Figure 3, at all altitudes in the NW Pacific, the model errors are a factor of 2–4 larger than the mean forecast errors. The global model transport error is obtained by applying the appropriate scaling factor from Figure 3 for each altitude bin to the global forecast errors. Examples of the resulting model errors are shown in Figure 4 for the upper and lower troposphere. Throughout much of the upper troposphere the model error is 10–20%. The largest model errors (exceeding 60%) in the free troposphere in the model are associated with the outflow of pollution from Asia across the Pacific Ocean. There are also large errors in the transport

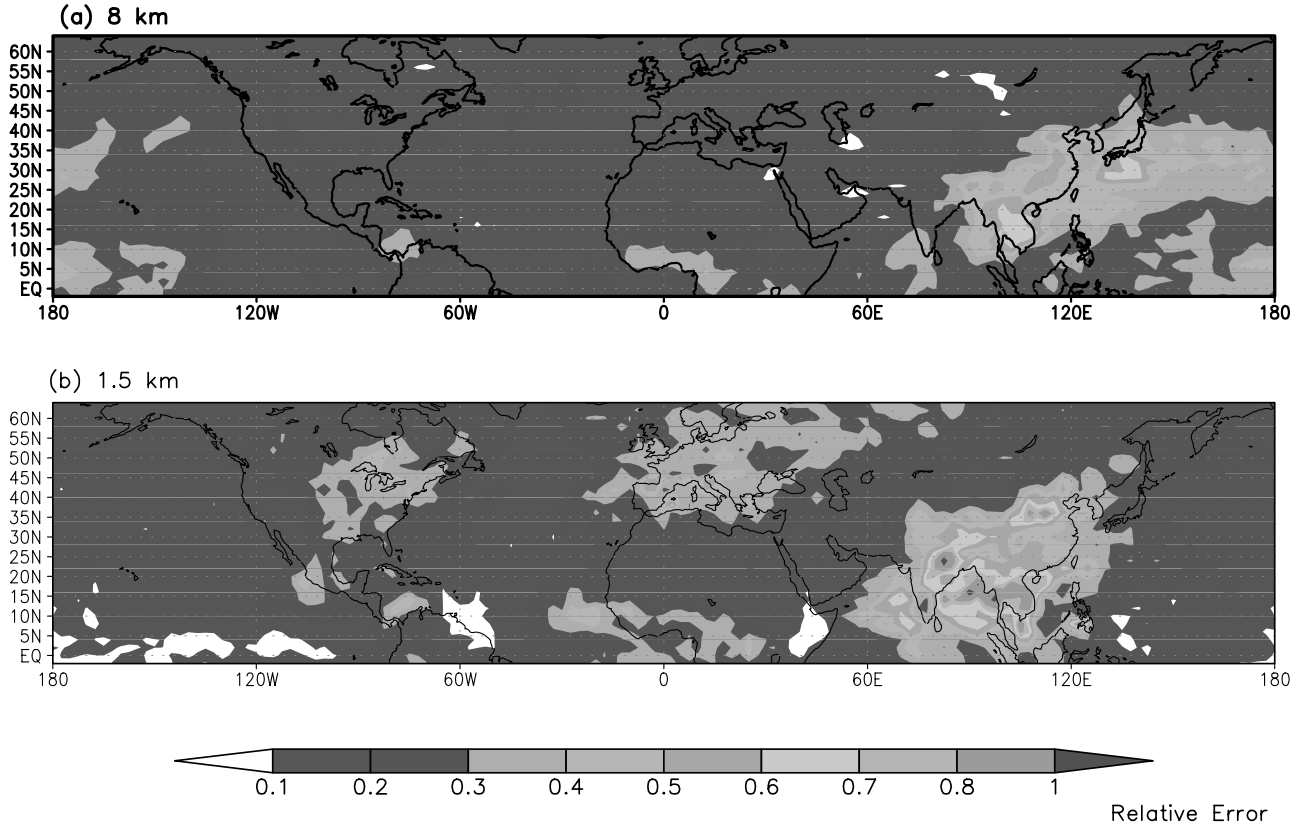

Figure 4. Relative model errors in (a) the upper troposphere (8 km) and (b) the lower troposphere (1.5 km) for the GEOS-CHEM model simulation of CO over the period February–April 2001. See color version of this figure at back of this issue.

of CO which has been convectively lofted into the free troposphere over South America and central Africa. In the lower troposphere the model errors are small (10–20%) in the remote troposphere but increase significantly over the continental source regions (where errors can be as large as 40–50%). The largest errors (exceeding 100%) are found over Southeast Asia. The model transport errors $\epsilon'^{j}_{\mathrm{mod}}$ (in equation (7)) are generated by sampling these error patterns along the TES orbit track and imposing a Gaussian distribution, with a mean of zero, with respect to the logarithm of the volume mixing ratio of CO.

[25] Examination of the forecast error covariance (not shown) reveals that the model transport errors have a horizontal correlation length scale of about 400 km, less than the distance between successive TES retrievals. Consequently, we assume that the model errors $\epsilon'^{j}_{\mathrm{mod}}$ are horizontally uncorrelated. The vertical correlation length scale in the free troposphere is 1–2 km, which is much smaller than the effective vertical correlation length scale of the TES retrievals (which provide about two pieces of information in the vertical profile). Therefore we also neglect vertical correlations in the model transport error.

5. Results

[26] The results of the inversion model using 8 days of pseudodata (2–16 March 2001) are shown in Figure 5 (red bars). The inversion model successfully estimates the true source strengths and significantly reduces the uncertainties for most of the sources. The a posteriori errors are less than 10% (compared with 50% for the a priori), with the exception of RWBB and RWFFBF, for which they are 10–25%. This is not unexpected since a large fraction of the emissions of CO from the latter two sources is in the Southern Hemisphere, while we restricted our inversion to the Northern Hemisphere. We find that in the absence of cloud contamination, comparable reduction in the source uncertainties can be achieved with about 4 days (2–8 March) of pseudodata.

[27] We examined the sensitivity of the inversion model to the added noise by repeating the inversion for 100 realizations of the noise in equation (7). We found that in each case the model accurately estimated the true source strengths. The mean a posteriori solution based on the statistics of all the solutions in the ensemble is similar to that shown in Figure 5, confirming the robustness of the results.

[28] The extent to which the inverse model can resolve the true state is given by the resolution matrix (the "averaging kernels" of the inversion) [*Rodgers*, 2000]

$$\mathbf{A}_{xx} = \mathbf{I} - \hat{\mathbf{S}}\mathbf{S}_a^{-1}, \tag{16}$$

where $\mathbf{I}$ is the identity matrix. Individual rows of the resolution matrix are plotted in Figure 6. The results show that, in general, the model resolves the individual sources well. The rows of the resolution matrix all have peak values close to unity for the corresponding source and are small elsewhere. From the resolution matrix we calculate that the degrees of freedom for signal (the number of independent pieces of information to constrain the nine-dimensional state

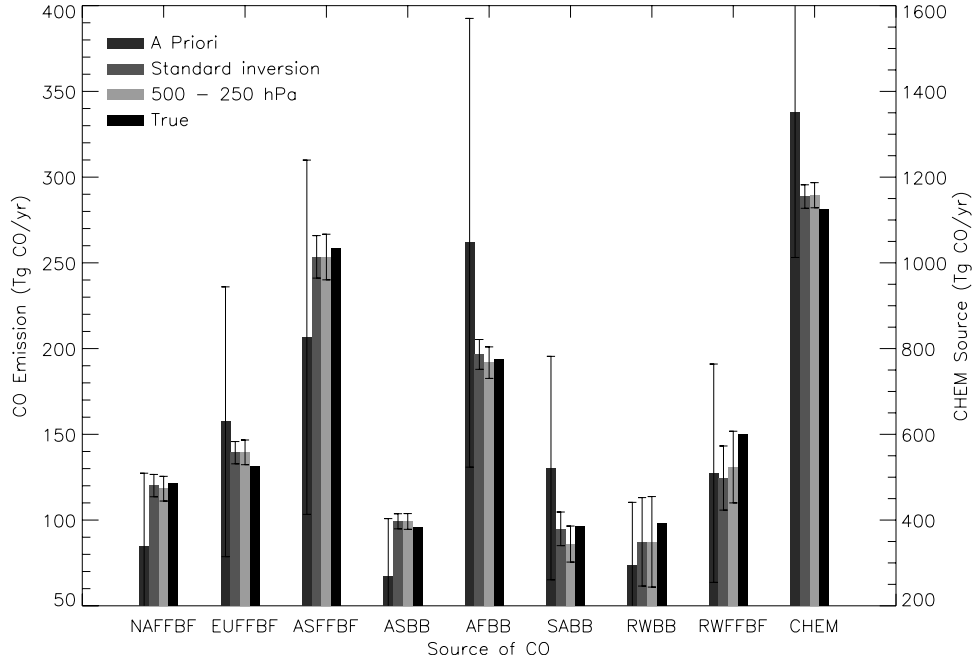

Figure 5. Comparison of a posteriori CO source estimates with true and a priori source strengths. Red bars indicate a posteriori source strengths estimated with instrument noise and model error, as described in section 3.2 (our standard inversion), green bars show a posteriori estimates obtained using only retrieval levels between 500 and 250 hPa. A priori source strengths are given by the blue bars, and the true source strengths are denoted by the black bars. Error bars indicate an uncertainty of 1-σ. See color version of this figure at back of this issue.

space) in the inversion is dofs = tr($\mathbf{A}_{xx}$) = 8.3. The inversion resolves the sources well (the dofs is close to 9) because the large-scale transport patterns of CO (as a result of the long lifetime of CO) are unique for the sources considered here and the TES observations provide dense sampling of these patterns. We find that even if we restrict the retrievals in the observation vector to levels above 500 hPa, the inversion analysis can estimate accurately the true source strengths (green bar in Figure 5). The dofs for this case is also 8.3.

[29] The sharply peaked kernels suggest that the TES observation vector constrains well the relatively coarse resolution state vector. They also imply that the nadir retrievals from TES have the potential to resolve CO source strengths on smaller geographical scales. However, recent inverse modeling studies have shown that there is still significant uncertainty associated with emissions on continental scales. For example, a posteriori estimates of biomass burning in Asia from the work of *Pétron et al.* [2002], *Kasibhatla et al.* [2002], and *Palmer et al.* [2003] differ by as much as a factor of 2. Additional constraints from TES would represent a significant improvement in our understanding of the global CO budget.

6. Summary and Discussion

[30] We have conducted an observing system simulation experiment for the TES satellite instrument to determine the potential of the instrument to constrain the magnitude of continental sources of CO. Using the GEOS-CHEM global three-dimensional chemical transport model we produced a pseudoatmosphere in which the relationship between the sources and concentrations of CO were known exactly. Nadir profile retrievals of CO from TES were generated by sampling this atmosphere along the TES orbit track. These pseudo-observations were incorporated into a maximum a posteriori inverse model to solve for the defined "true" source strengths. We focused on constraining a 9-element state vector representing CO source strengths from different regions and processes.

[31] Because the GEOS-CHEM model was used as the forward model in the inversion as well as to generate the pseudo-observations, it was necessary to independently characterize the errors in the GEOS-CHEM simulation of CO and add these errors to the forward model simulation. A previous study, by *Palmer et al.* [2003], quantified the GEOS-CHEM transport error for CO over the NW Pacific by simulation of aircraft observations from the NASA TRACE-P mission (Febuary–April 2001). We extrapolated these errors globally by using GEOS-CHEM chemical forecasts of CO and the NMC method [*Parish and Derber*, 1992], in which it is assumed that differences between forecasts valid for the same end point in time, but of different lengths, are representative of the forecast error structure in the model. We constructed the global transport error pattern based on the statistics of 89 pairs of 48- and 24-hour forecasts of CO that were generated with GEOS-CHEM during the TRACE-P mission in February–April 2001. The global forecast error patterns were then scaled to match the model errors obtained by *Palmer et al.* [2003] over the NW Pacific. This approach represents an advance over previous methods of characterizing forward model errors in chemical inversions. It demonstrates the utility of complementary aircraft observations when interpreting satellite observations.

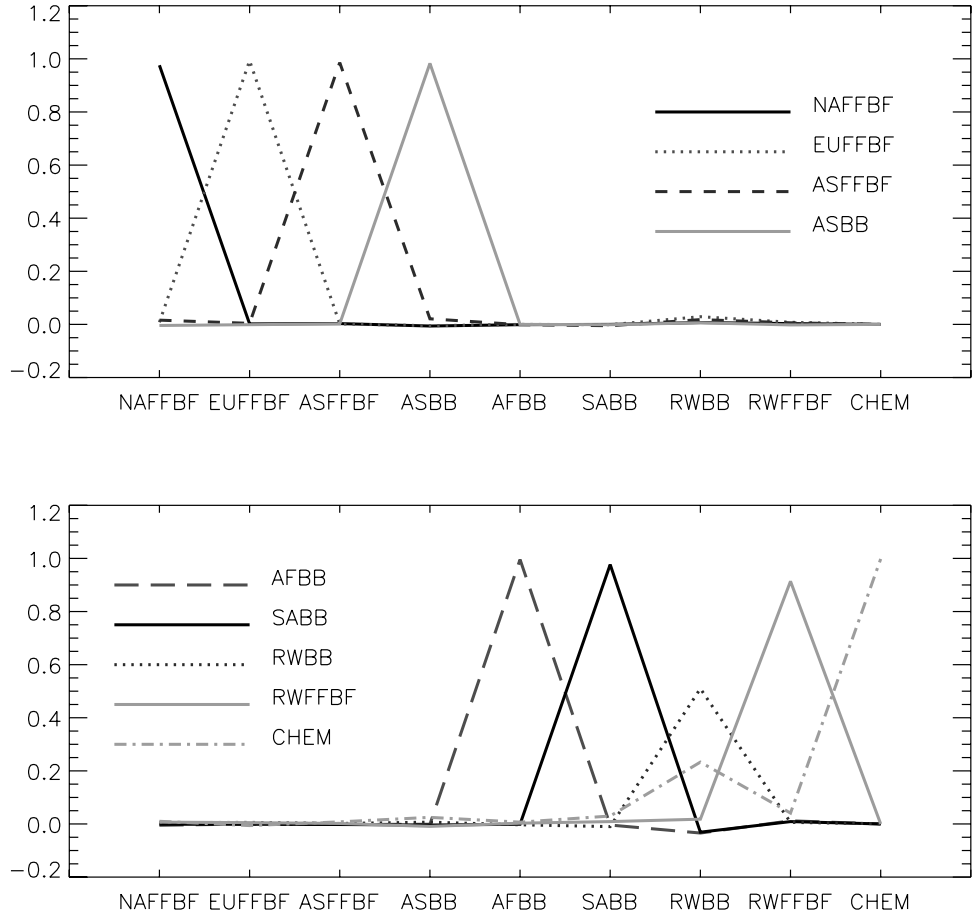

Figure 6. Resolution matrix for the inversion. Each line represents a row of the matrix (for which the corresponding source is indicated in the legend) and describes the sensitivity of the a posteriori source to the true state. These are not continuous functions, but for clarity we have plotted them as such. See color version of this figure at back of this issue.

[32] Using our best estimates of model errors and instrument noise, we found that the inversion analysis accurately estimated the true source strengths and significantly reduced uncertainty in the sources, starting from randomly chosen a priori estimates of the sources. A posteriori uncertainties on the sources were typically less than 10% as compared to 50% assumed for the a priori. This suggests that the TES nadir retrievals of CO have the potential to constrain accurately estimates of the CO continental source strengths. We focused here on continental sources; however, our results indicate that TES observations should contain sufficient information to help quantify CO sources on smaller geographical scales. This will be the focus of future work.

[33] Proper error characterization will be crucial to fully exploit the information in the TES retrievals. The success of the pseudo-observations in constraining the estimate of the sources in our analysis was contingent on the errors added to the inversion analysis being perfectly characterized and free of biases or systematic errors. *Kasibhatla et al.* [2002] found that their inversion was relatively insensitive to a globally uniform bias of 20% in the OH abundance (the globally averaged abundance of OH is known to within 10–20%). The presence of large regional biases, however, either in the retrieval or in the forward model (as a result of errors in transport or in the chemistry), will strongly impact the inversion. Our results indicate that proper error characterization must be an essential component of inversion analyses using satellite observations.

Appendix A: Sequential Update

[34] Although we restrict the observations to between 0°N and 60°N and from the surface to 250 hPa, the large data volume makes the size of the Jacobian matrix and the observation error covariance matrix computationally cumbersome. We therefore use a sequential update approach in solving equation (12). We sequentially update the estimate of the state vector by ingesting one profile $\hat{\mathbf{y}}^j$ and one observational error covariance matrix $\mathbf{S}_\varepsilon^j$ at a time. The sequential update is described by the following algorithm:

$\delta\mathbf{x}_0 = \mathbf{x}_a - \mathbf{x}_i$

$\mathbf{S}_0 = \mathbf{S}_a$

do $j = 1$ to m

$$\mathbf{S}_j = \left[\left(\mathbf{K}^j\right)^T\left(\mathbf{S}_\varepsilon^j\right)^{-1}\mathbf{K}^j + \left(\mathbf{S}_{j-1}\right)^{-1}\right]^{-1} \tag{A1}$$

$$\delta\mathbf{x}_j = \mathbf{S}_j\left[\left(\mathbf{K}^j\right)^T\left(\mathbf{S}_\varepsilon^j\right)^{-1}\left(\hat{\mathbf{y}}^j - \mathbf{F}^j(\mathbf{x}_i)\right) + \mathbf{S}_{j-1}^{-1}\delta\mathbf{x}_{j-1}\right] \tag{A2}$$

enddo

$$\mathbf{x}_{i+1} = \mathbf{x}_i + \delta\mathbf{x}_m,$$

where m is the total number of individual profiles in the data set, $\mathbf{K}^j$ is the sensitivity of the observations in the jth profile to the sources $\mathbf{x}_i$, and $\mathbf{S}_\varepsilon^j$ is the observation error covariance matrix of the jth profile. Note that the observation error covariance matrix in equation (12) must be block diagonal, with elements given by equation (8) (which are uncorrelated between locations j), for the sequential update to be a valid implementation of equation (12).

[35] **Acknowledgments.** We thank Prasad Kasibhatla for useful discussions. This work was supported by the NASA Atmospheric Chemistry Modeling and Analysis Program (ACMAP) and the California Institute of Technology President's Fund.

References

Beer, R., T. A. Glavich, and D. M. Rider, Tropospheric Emission Spectrometer for the Earth Observing System's Aura satellite, *Appl. Opt.*, *40*, 2356–2367, 2001.

Bergamaschi, P., R. Hein, M. Heimann, and P. J. Crutzen, Inverse modeling of the global CO cycle: 1. Inversion of CO mixing ratios, *J. Geophys. Res.*, *105*, 1909–1927, 2000a.

Bergamaschi, P., R. Hein, M. Heimann, and P. J. Crutzen, Inverse modeling of the global CO cycle: 2. Inversion of $^{13}C/^{12}C$ and $^{18}O/^{16}O$ isotope ratios, *J. Geophys. Res.*, *105*, 1929–1945, 2000b.

Bey, I., M. G. Schultz, D. J. Jacob, R. M. Yantosca, J. A. Logan, B. D. Field, A. M. Fiore, Q. Li, H. Y. Liu, and L. J. Mickley, Global modeling of tropospheric chemistry with assimilated meteorology: Model description and evaluation, *J. Geophys. Res.*, *106*(D9), 23,073–23,096, 2001a.

Bey, I., D. J. Jacob, J. A. Logan, and R. M. Yantosca, Asian chemical outflow to the Pacific: Origins, pathways and budgets, *J. Geophys. Res.*, *106*, 23,097–23,113, 2001b.

Bowman, K. W., J. Worden, T. Steck, H. M. Worden, S. Clough, and C. Rodgers, Capturing time and vertical variability of tropospheric ozone: A study using TES nadir retrievals, *J. Geophys. Res.*, *107*(D23), 4723, doi:10.1029/2002JD002150, 2002.

Clerbaux, C., J. Hadji-Lazaro, D. Hauglustaine, G. Megie, B. Khattatov, and J.-F. Lamarque, Assimilation of carbon monoxide measured from satellite in a three-dimensional chemistry-transport model, *J. Geophys. Res.*, *106*, 15,385–15,394, 2001.

Clough, S. A., and M. J. Iacono, Line-by-line calculation of atmospheric fluxes and cooling rates: 2. Application to carbon dioxide, ozone, methane, nitrous oxide and the halocarbons, *J. Geophys. Res.*, *100*, 16,519–16,535, 1995.

Clough, S. A., C. P. Rinsland, and P. D. Brown, Retrieval of tropospheric ozone from simulations of nadir spectral radiances as observed from space, *J. Geophys. Res.*, *100*, 16,579–16,593, 1995.

Clough, S. A., J. R. Worden, P. D. Brown, M. W. Shephard, C. P. Rinsland, and R. Beer, Retrieval of tropospheric ozone from simulations of nadir spectral radiances from space, *J. Geophys. Res.*, *107*(D21), 4589, doi:10.1029/2001JD001307, 2002.

Derber, J., and F. Bouttier, A reformulation of the background error covariance in the ECMWF global data assimilation system, *Tellus, Ser. A*, *51*, 195–221, 1999.

Drummond, J. R., and G. S. Mand, The Measurements of Pollution in the Troposphere (MOPITT) instrument: Overall performance and calibration requirements, *J. Atmos. Oceanic Technol.*, *13*, 314–320, 1996.

Duncan, B. N., R. V. Martin, A. C. Staudt, R. Yevich, and J. A. Logan, Interannual and seasonal variability of biomass burning emissions constrained by satellite observations, *J. Geophys. Res.*, *108*(D2), 4040, doi:10.1029/2002JD002378, 2003.

Heald, C. L., D. J. Jacob, P. I. Palmer, M. J. Evans, G. W. Sachse, H. B. Singh, and D. R. Blake, Biomass burning emission inventory with daily resolution: Application to aircraft observations of Asian outflow, *J. Geophys. Res.*, *108*(D21), 8811, doi:10.1029/2002JD003082, 2003a.

Heald, C. L., et al., Asian outflow and trans-Pacific transport of carbon monoxide and ozone pollution: An integrated satellite, aircraft, and model perspective, *J. Geophys. Res.*, *108*, doi:10.1029/2003JD003507, in press, 2003b.

Jacob, D. J., J. H. Crawford, M. M. Kleb, V. S. Connors, R. J. Bendura, J. L. Raper, G. W. Sachse, J. C. Gille, L. Emmons, and C. L. Heald, Transport and Chemical Evolution over the Pacific (TRACE-P) aircraft mission: Design, execution, and first results, *J. Geophys. Res.*, *108*(D20), 8781, doi:10.1029/2002JD003276, 2003.

Kasibhatla, P., A. Arellano, J. A. Logan, P. I. Palmer, and P. Novelli, Top-down estimate of a large source of atmospheric carbon monoxide associated with fuel combustion in Asia, *Geophys. Res. Lett.*, *29*(9), 1900, doi:10.1029/2002GL015581, 2002.

Lamarque, J.-F., B. Khattatov, J. C. Gille, and G. P. Brasseur, Assimilation of MAPS CO in a global three-dimensional model, *J. Geophys. Res.*, *104*, 26,209–26,218, 1999.

Luo, M., R. Beer, D. J. Jacob, J. A. Logan, and C. D. Rodgers, Simulated observation of tropospheric ozone and CO with the Tropospheric Emission Spectrometer (TES) satellite instrument, *J. Geophys. Res.*, *107*(D15), 4270, doi:10.1029/2001JD000804, 2002.

Palmer, P. I., D. J. Jacob, D. B. A. Jones, C. L. Heald, R. M. Yantosca, J. A. Logan, G. W. Sachse, and D. G. Streets, Inverting for emissions of carbon monoxide from Asia using aircraft observations over the western Pacific, *J. Geophys. Res.*, *108*(D21), 8828, doi:10.1029/2003JD003397, 2003.

Papoulis, A., *Probability, Random Variables and Stochastic Processes*, McGraw-Hill, New York, 1984.

Parish, D. F., and J. C. Derber, The National Meteorological Center's spectral statistical interpolation analysis system, *Mon. Weather Rev.*, *120*, 1747–1763, 1992.

Pétron, G., C. Granier, B. Khattatov, J.-F. Lamarque, V. Yudin, J.-F. Muller, and J. Gille, Inverse modeling of carbon monoxide surface emissions using Climate Monitoring and Diagnostics Laboratory network observations, *J. Geophys. Res.*, *107*(D24), 4761, doi:10.1029/2001JD001305, 2002.

Rabier, F., A. McNally, E. Andersson, P. Courtier, P. Unden, J. Eyre, A. Hollingsworth, and F. Bouttier, The ECMWF implementation of three-dimensional variational assimilation (3D-var), II, Structure functions, *Q. J. R. Meteorol. Soc.*, *124*, 1809–1829, 1998.

Reichle, H. G., et al., Space shuttle based global CO measurements during April and October 1994, MAPS instrument, data reduction, and data validation, *J. Geophys. Res.*, *104*, 21,443–21,454, 1999.

Rodgers, C. D., *Inverse Methods for Atmospheric Sounding: Theory and Practice*, World Sci., River Edge, N. J., 2000.

Yevich, R., and J. A. Logan, An assessment of biofuel use and burning of agricultural waste in the developing world, *Global Biogeochem. Cycles*, *17*(4), 1095, doi:10.1029/2002GB001952, 2003.

I. Bey, Swiss Federal Institute of Technology (EPFL), 1015 Lausanne, Switzerland.

K. W. Bowman and J. R. Worden, California Institute of Technology, Jet Propulsion Laboratory, 4800 Oak Grove Drive, Pasadena, CA 91109, USA.

R. N. Hoffman, Atmospheric and Environmental Research, Inc., 131 Hartwell Avenue, Lexington, MA 02421, USA.

D. J. Jacob, D. B. A. Jones, P. I. Palmer, and R. M. Yantosca, Division of Engineering and Applied Sciences and Department of Earth and Planetary Sciences, Harvard University, Pierce Hall, 29 Oxford Street, Cambridge, MA 02138, USA. (dbj@io.harvard.edu)

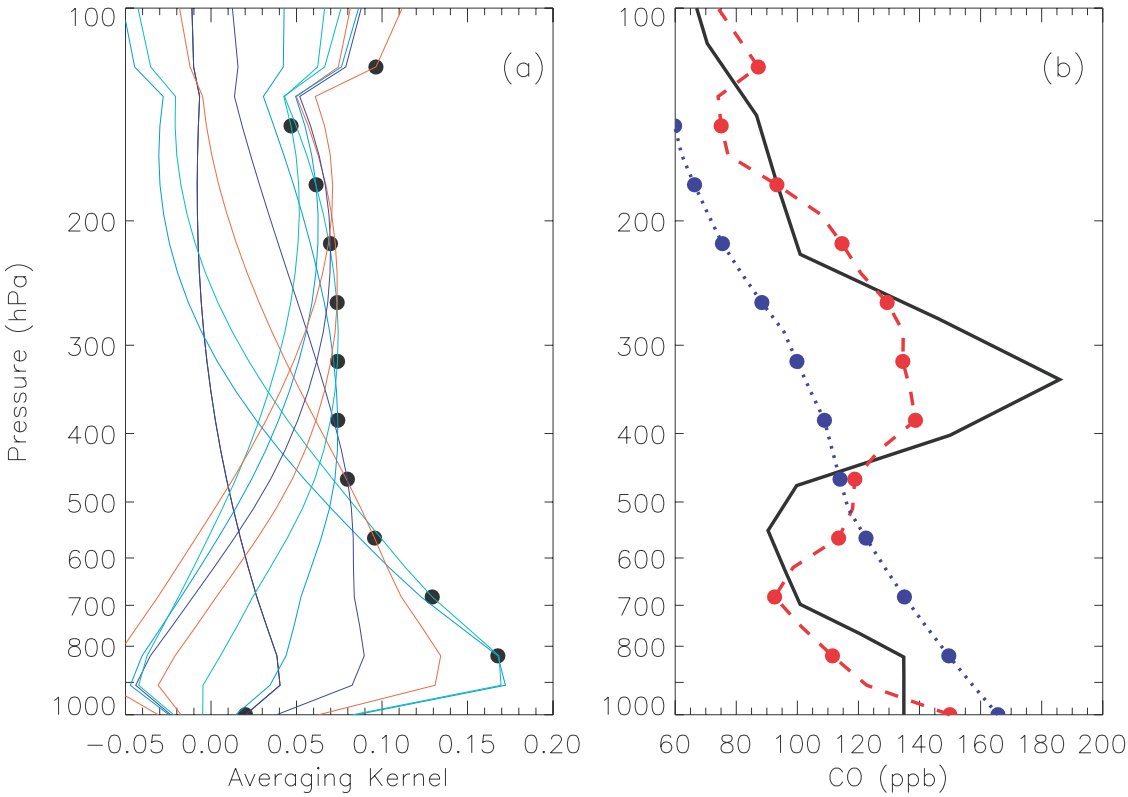

Figure 1. (a) Averaging kernels for TES nadir retrieval of CO for selected retrieval levels between 1000 and 100 hPa. The corresponding retrieval levels for the individual averaging kernels are indicated by solid circles. (b) Example of a retrieved profile. The true profile is represented by the solid line, the a priori profile is shown by the dotted line, and the retrieved profile is denoted by the dashed line. The retrieval levels are indicated by the solid circles.

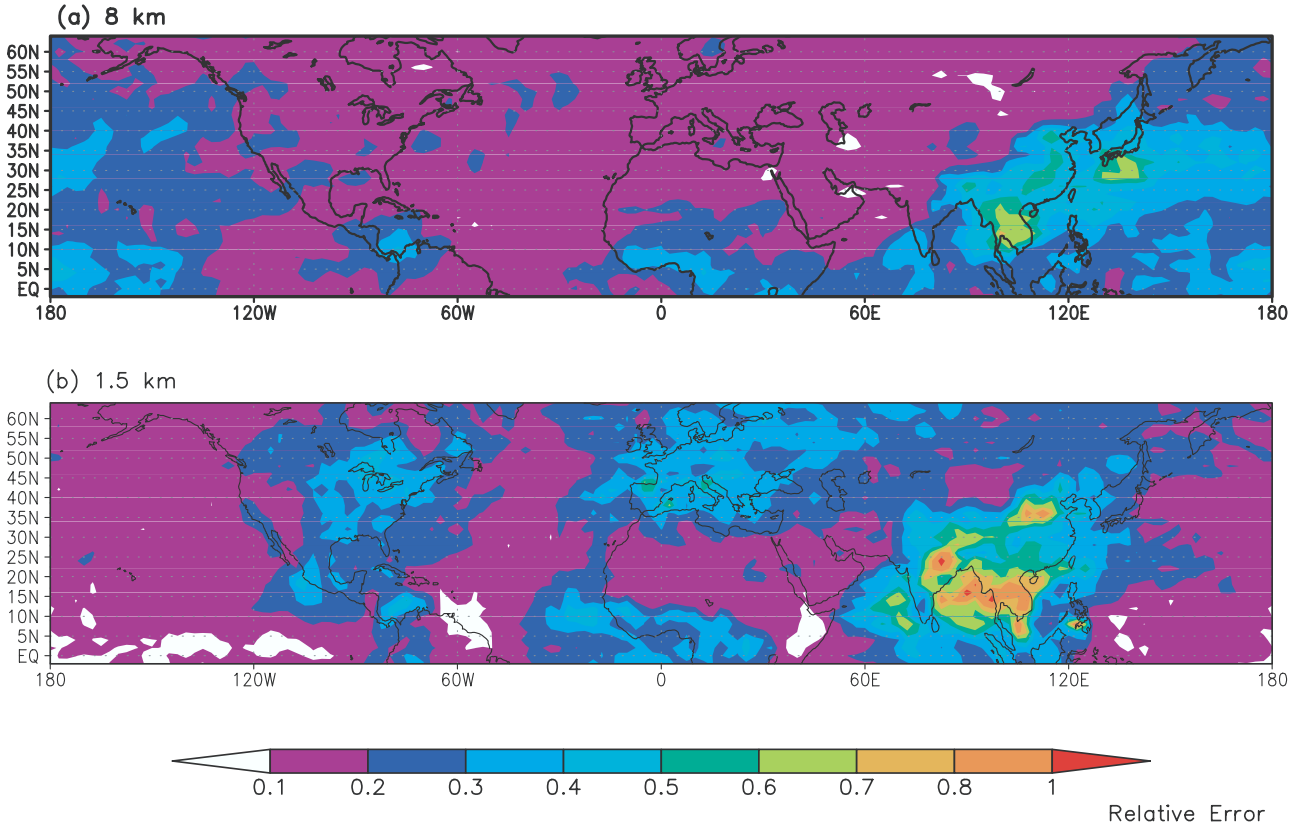

Figure 4. Relative model errors in (a) the upper troposphere (8 km) and (b) the lower troposphere (1.5 km) for the GEOS-CHEM model simulation of CO over the period February–April 2001.

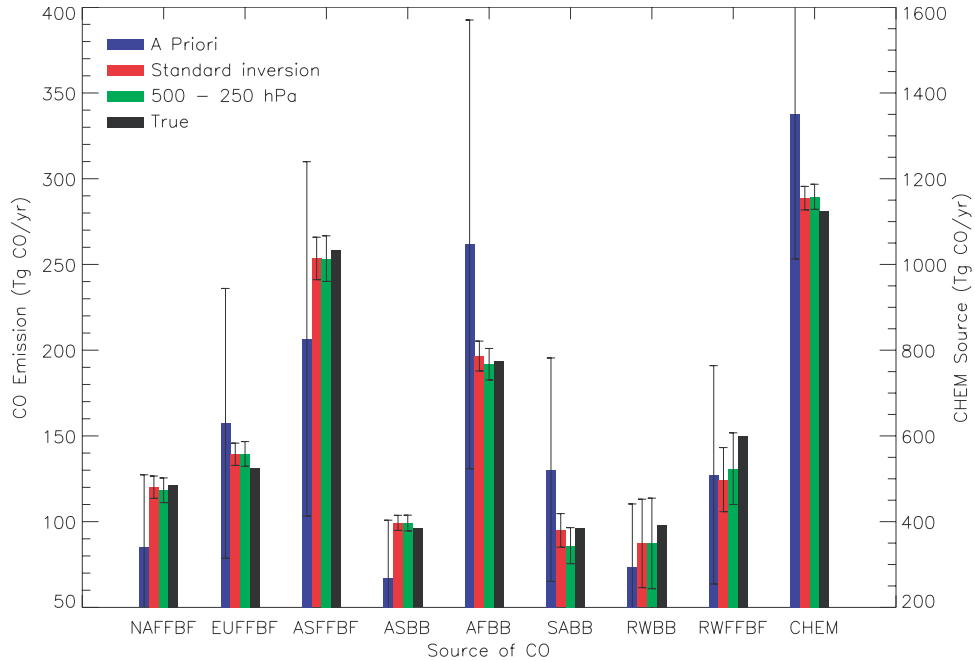

Figure 5. Comparison of a posteriori CO source estimates with true and a priori source strengths. Red bars indicate a posteriori source strengths estimated with instrument noise and model error, as described in section 3.2 (our standard inversion), green bars show a posteriori estimates obtained using only retrieval levels between 500 and 250 hPa. A priori source strengths are given by the blue bars, and the true source strengths are denoted by the black bars. Error bars indicate an uncertainty of 1-σ.

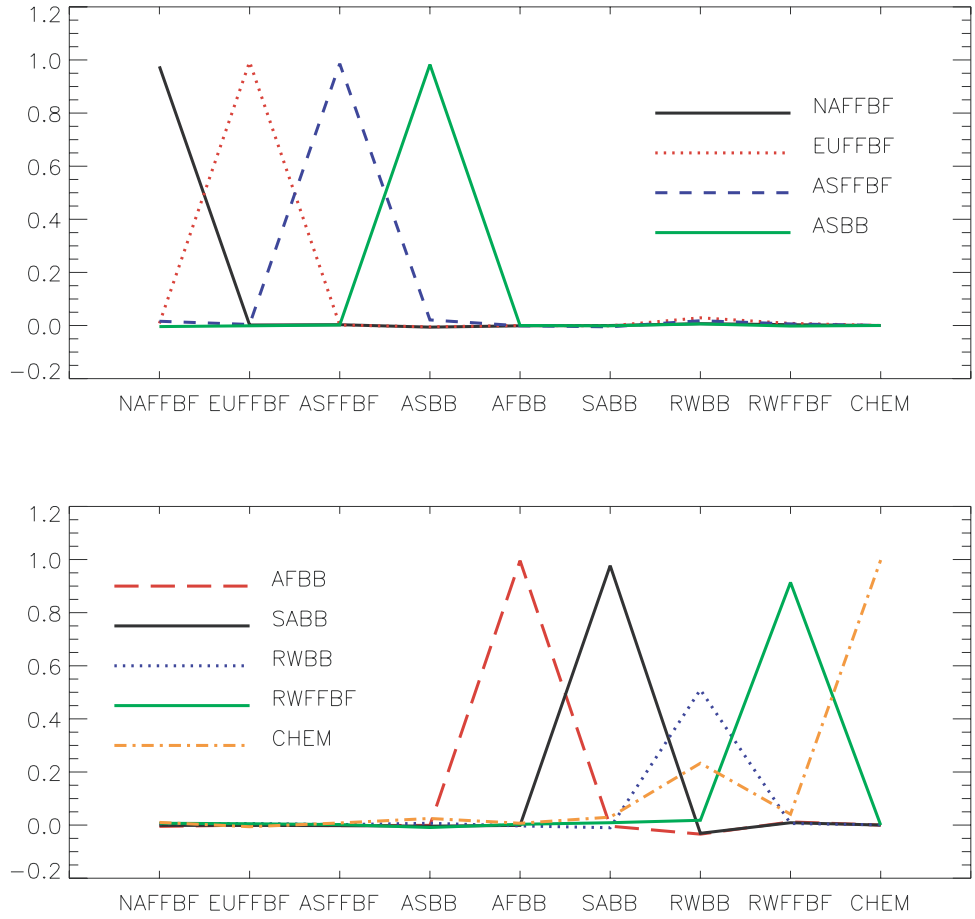

Figure 6. Resolution matrix for the inversion. Each line represents a row of the matrix (for which the corresponding source is indicated in the legend) and describes the sensitivity of the a posteriori source to the true state. These are not continuous functions, but for clarity we have plotted them as such.